ELSEVIER

Biophysical Chemistry 124 (2006) 52–61

Biophysical Chemistry

http://www.elsevier.com/locate/biophyschem

Potential of cadmium sulphide nanorods as an optical microscopic probe to the folding state of cytochrome *C*

Shibsekhar Roy [a], Soumitra Kar [b], Subhadra Chaudhuri [b], Anjan Kr Dasgupta [a,*]

[a] *Dept of Biochemistry, University of Calcutta, 35-Ballygunge Circular Road, Kolkata-700019, India*
[b] *Department of Material Sciences, Indian Association for the Cultivation of Science, Kolkata 700032, India*

Received 29 March 2006; received in revised form 12 May 2006; accepted 12 May 2006
Available online 30 June 2006

Abstract

The folding behavior of cytochrome *C* (Cyt-C) conjugated with CdS nanorods (CdSnr) is amenable to monitoring by bright field microscopy, the porosity and percolating behavior of such protein conjugated nanoclusters depending on the folding history prior to the conjugation. The method has been used to predict the thermal melting behavior as well as guanidine hydrochloride induced unfolding of Cyt-C. Dynamic light scattering studies indicate that the size distribution of the nanoforms widens in presence of the protein. Furthermore, there is emergence of clusters with higher conductivity and altered zeta potential. Increase of second virial coefficient of CdS nanoforms in the presence of Cyt-C (obtained from static light scattering experiments) implies presence of protein coat over the hydrophobic nanosurface. The results are supported by morphological changes observed through scanning electron microscopy (SEM). Accordingly, the X-ray diffraction pattern shows a change of crystallographic orientations of CdSnr in presence of Cyt-C.

Keywords: Cadmium sulphide nanoforms; Cytochrome *C*; Folding; Dynamic light scattering; Second virial coefficient; Static light scattering; Scanning electron microscopy; X-ray diffraction

1. Introduction

Cyt-C is a very much physiologically important small (MW 13.2 kDa) globular protein residing in the inner membrane space of mitochondria, which plays the key role of electron transfer from complex 3 to complex 4 of electron transport chain during oxidative phosphorylation. The folding pathway of this protein has been of much interest for understanding of the diverse time scale of the process as well as the correlation between structural and functional dynamics. Both small [1] and large time scale [2] of folding has been reported for protein folding pathway. In case of Cyt-C, both fast [3,4] and slow [2] kinetics have been reported. In our previous work [5] also, we have shown a slow unfolding kinetics and a strong correlation between heme peroxidase activity and conformational dynamics during a deaggregatory-folding pathway. The heme binding amino acids (cystine residues with thio-ethar linkage) play a key role in this folding [6], where both coordinate and the covalent attachment of heme to protein through two thio-ether bonds to a Cys–Xaa–Xaa–Cys–His peptide motif [7] are present. The role of heme group during folding (or unfolding) process [8] has been assigned to be very important for its interaction with various peptide moieties and that is why heme serves as a natural indicator of the folding state [9]. Even heme group helps in globin chain assembly [10] by showing chaperon like activity. The his-heme misligation and proline mis-isomerisation [11] induced aggregatory unfolding process and the reverse pathway, i.e. deaggregatory folding process is characterized by various intermediate states, which we have shown by the coherent study of population heterogeneity and peroxidase activity [5]. Besides ligation, a large population of unfolding induced altered compact structures forms some hydrophobic core to impart more diversity in the unfolding process [12]. The probable physiological role of the cooperative nature of folding pathway in that work has been helpful to explain the link between electron transfer and alteration of folding pathway of Cyt-C(I) [13].

With the emergence of nanotechnology, the physiological aspect of protein-nanoparticle interaction is becoming very

* Corresponding author.
E-mail address: adgcal@gmail.com (A.K. Dasgupta).

0301-4622/$ - see front matter © 2006 Published by Elsevier B.V.
doi:10.1016/j.bpc.2006.05.011

important as the potential of nanoparticle as a sensor of the protein's conformation is gaining momentum. Study of protein nanoparticle interaction has recently found much importance due to mainly two reasons; firstly, in medicinal industry for developing biosensors or creating site targeted drug delivery system and, secondly, to assess the mode of nanotoxicity. Nanoparticles reside as clusters in solution. The self-assembly of the nanoparticles leads to the formation of superstructures of varying order on the linear arrays [14]. Gold nanoparticle mediated colorimetric reporting of the unfolding of Cyt-C has recently [15] thrown light to the interaction between nanosurface and protein conformation. The concentration dependent colloidal gold particle mediated unfolding of Cyt-C has been observed by circular dichroism, UV–visible and infrared spectroscopy [16]. Again, the interaction between apo Cyt-C and sulphonated polystyrene has also been observed [17] resulting in large size complex of the positively charged protein. This electrostatic mode of protein nanosurface interaction has been shown to vary with the surface charge of nanosurface as well as the protein [18]. In addition, high resolution 2-D 1H–15N NMR has shown structural alteration up to amino acid resolution in presence of nanoparticle [19]. The two-dimensional NMR analysis also shows an ensemble of protein molecules with near-native conformations to show the conformational alteration of protein due to surface adsorption [20]. A large amount of nanoparticle systems show slow relaxation kinetics of energy fluctuations depending on the solvent interaction, which has shown a complex non-exponential relaxation dynamics for myoglobin-metal nanocluster system [21]. This electrochemical fluctuation may well be reflected on the varying degree of charge dependent interaction with the surface of the protein. The electrical properties like zeta potential, conductance are now being in use to characterize the electrochemical properties of the nanosurface [22,23] to determine the charge dependent attraction and repulsion properties of nanoparticle system. Hence, size and charge based population distributions are good representatives of the properties of nanoclusters.

The peroxidase activity being the reflection of folding state of heme protein, like Cyt-C, this property may well be the primary target to compare various folding pathways as well as to verify the influence of the nanosurface on the folding state of the protein. Even, efforts are on to construct CdS made biosensor by assaying peroxidase activity [24]. The active state of the protein denotes the distribution of its energy state during enzymatic activity. Any perturbation on the energy state due to protein–nanoparticle interaction (like perturbation in the HOMO–LUMO energy gap [22]) may result in the alteration of their surface charge distribution, which may be reflected on the enzymatically active state distribution during peroxidase activity profile of the protein.

The solution properties of protein are also measured by static light scattering methods to understand protein's self interaction [25] as well as protein–protein interaction [26] by obtaining the second virial coefficient of the Debye plot of the system. We have used this method to measure the nature and order of protein nanoparticle complex formation.

In this paper, we report a novel but simple way of tracing the folding route of Cyt-C. The method has an inherent robustness, as it provides a visually enabled way to trace the folding pathway of the protein. Unlike the color method used by Chah et al. [15] in which the folding states were probed using color difference of gold nanoparticles, this provides a simpler clustering method, which can be monitored even by using bright field microscopy in addition to light scattering and other sophisticated studies. In this study, we have used cadmium sulphide nanorods (CdSnr) as probe for its higher sensitivity towards protein. The reason behind choosing this nanoform is its unique dimension. Its diameter is around 35 nm and its length is about a micron. This length is of special advantage as it can easily be detectable by optical microscopy. As CdS is known for its luminescent properties, to ascertain the absence of any optical interference, we have kept uniform illumination throughout the experiment. For a comparative study of protein–nanoform interaction, we have also used cadmium sulphide nanoparticles (CdSnp).

2. Materials

2.1. Preparation of protein solution

Horse heart cytochrome *C* has been purchased from Sigma Aldrich (C 7752). The stock protein solution is prepared in 50 mM phosphate buffer of pH 7.4. The stock concentration was taken as 5 mg/ml, i.e. 400 μM.

2.2. Reagent preparation for peroxidase activity

The substrate *o*-dianisidine has been purchased from Sigma Aldrich (D3252). The solution was prepared as 5 mg/ml concentration of *o*-dianisidine in methanol/sodium acetate [(0.25 M), pH 5.0, 3:7 (v/v)]. Hydrogen peroxide stock was prepared at a concentration of 0.3% in double distilled water.

2.3. Preparation of denaturant solution

Guanidine hydrochloride has been purchased from SRL (Sisco Research Laboratory).

The stock has been prepared at a concentration of 8 M.

3. Methods

3.1. Preparations of CdS nanoparticles and nanorods

The CdS nanostructures were prepared separately by using a solvothermal technique [27]. The preparation of CdS nanostructures was performed in a closed cylindrical Teflon-lined stainless steel chamber. For nanoparticles ($d \sim 7.5$ nm), ethylene glycol was used as the solvent whereas for the nanorods ($d \sim 35$ nm and length ~ 1 μm) ethylenediamine was used. Nanoforms prepared this way have been used to interact with Cyt-C (mainly in 1:1 stoichiometry). For experiments with protein, a mass ratio 1:1 is generally used. In case of 1:1, both the nanoforms and protein were kept at concentration (0.1 mg/ml).

3.2. Refolding study

3.2.1. Preparing the protein solutions for activity assay

At first, 20 μM Cyt-C has been unfolded by 8 M Gdn–HCl and incubated for an hour.

The unfolded protein solution is diluted 100 times with the 50 mM phosphate buffer (pH 7.4). Hence, Cyt-C concentration becomes 200 nM.

3.2.2. Preparation of solution for unfolding and folding kinetics

For the comparison between folding and unfolding course of Cyt-C, CdSnr treated Cyt-C (1:1 weight ratio) solution was unfolded in 1, 3 and 6 M Gdn–HCl concentration and for the refolding purpose the 8 M Gdn–HCl treated unfolded protein solutions were diluted such a way that resultant protein and CdSnr concentration are 0.2 mg/ml for each unfolded and folded solution to omit any influence of concentration effect.

3.2.3. Activity assay

For the assay of the peroxidase activity for different refolding states of the protein, the *o*-dianisidine assay has been performed with standard protocol [28–30]. Peroxidase activity of heme can be used for probing heme proteins with high degree of sensitivity. The activity kinetics was assayed spectrophotometrically by Diode Array spectrophotometer Analytik Jena (spekol 1200) and its dynamics was studied in different time intervals of the spectra. The absorbance kinetics was studied at 460 nm (for oxidized *o*-dianisidine) to calculate the specific activity from the slope of the reaction.

3.3. Dynamic light scattering

3.3.1. Size measurement

The Nano-ZS (Malvern) instrument we have used for our experiment is equipped with a 4 mW He–Ne Laser (λ=632 nm). The sample is poured in a 3 ml glass cuvette (path length 1 cm) with all transparent walls. Prior to the DLS study, protein samples were filtered through a 2 μm membrane filter (Acrodisc). The operating procedure was programmed (using the DTS software supplied with the instrument) such that there are average 20 runs, each being averaged for 10 s, and a particular Rh is computed in each case and ultimately the result is presented as the distribution of Rh. In DLS, one intends to measure the three dimensional pdf (probability distribution function) for diffusion process P, a general expression is given by

$$P(r,t|0,0) = (4\pi Dt)^{-3/2}\exp(-r^2/4Dt) \tag{1}$$

Since this function only depends on D, the diffusion constant of the system, this allows us to obtain the value for the Stokes radius Rh=a, if the pdf can be measured. The Stokes relation can compute the diameter of the scattering particle,

$$D = \frac{F}{6\pi\eta a} \tag{2}$$

The link between the pdf and the power spectrum is a consequence of the translation of the relative motion of the scattering particles in to phase differences of the scattered light. So, if $I(t)$ is the intensity of the scattered light, then autocorrelation function $C(\tau)$ satisfying,

$$C(\tau) \sim \langle I(t)\ I(t+\tau)\rangle.$$

The correlation function undergoes an exponential decay with time,

$$C(\tau) \sim \exp(-\tau/D) \tag{3}$$

It is then straightforward to measure the diffusion coefficient D from the slope of the log C–τ plot. This (D) in turn provides the hydrodynamic size (d_h) follows from the Stokes' relation. A particular d_h is evaluated several times and the result is presented in terms of a distribution of the hydration diameter. The instrument provided the size distribution in (a) intensity mode, (b) volume mode and (c) number mode. While the first, providing the size distribution of scattered intensity is more sensitive to alteration in d_h (intensity varying as $\sim d_h^6$), the second and third mode provide size distribution of volume and number of particles respectively in the light path. For monitoring the population of aggregates (whose numbers are appreciably high in some cases), the multimode intensity distribution was used.

3.3.2. Zeta potential measurement by laser Doppler velocimetry (LDV)

The same instrument Zetasizer nano calculates the zeta potential. In an ionic solution, the development of a net charge on the surface of a particle alters the ionic distribution in the interfacial region, which results in the increase in counter ion concentration close to the surface. Thus, an electrical double layer exists surrounding each particle. The inner part of the layer, i.e. the Stern layer, is characterized by strongly bound ions and the outer layer consists of loosely bound diffusing ions. Within this diffusive layer, the ions as well as particles form a stable entity confined by a boundary. With the gravity induced particle movement, ions within that boundary also move along it but not the ions beyond this boundary. The potential existing in this boundary is called the zeta potential.

This is to be remembered that zeta potential is purely an electro kinetic property of the electrical double layer surrounding the subject but not the surface of the subject itself. This quantity is measured by determining the electrophoretic mobility and then applying the value in Henry's equation. The velocity of a particle in an electric field is known as electrophoretic mobility (U_E). Now, applying this value to Henry's equation, we will obtain the value of zeta potential (z).

$$z = \frac{3\eta U_E}{2\varepsilon \cdot f(K_a)} \tag{4}$$

where η=viscosity, ε=dielectric constant and $f(K_a)$=Henry's function.

A special capillary cell is used for this measurement with embedded electrodes at either of the two ends. Particles move towards the electrode of the opposite charge and their velocity is measured and expressed in unit field strength as their mobility.

Now, the technique that is used for this measurement is laser Doppler velocimetry. This technique efficiently measures the velocity of tiny particles within the fluid streams moving at the velocity of the fluid. The receiving optics is focused so as to relay the scattering particles in the cell. After being scattered at an angle of 17°, the beam is combined with the scattered beam and produces a fluctuating signal, whose fluctuation rate is proportional to the particle velocity. Then a signal processor extracts the characteristic frequency of the scattered light.

3.4. Static light scattering (SLS) measurements

The same instrument Zetasizer Nano is used in the different mode (static light source) to perform these experiments. The Rayleigh equation describes the intensity of light scattered from a particle in a solution

$$\frac{KC}{R_\theta} = \left(\frac{1}{M} + 2 \cdot a_2 \cdot C\right) \cdot P(\theta) \tag{5}$$

where K=optical constant, C=concentration, R_θ=the Rayleigh ratio, M=molecular weight, a_2=second virial coefficient and $P(\theta)$=scattering angle.

In practice, the particle sizes being too small in comparison to the wave length of the scattered light the value of $P(\theta)$ reduces to 1 and the equation becomes

$$\frac{KC}{R_\theta} = \left(\frac{1}{M} + 2 \cdot a_2 \cdot C\right) \tag{6}$$

Normally, this equation is exploited to measure the molecular weight of a particle in solution and the associated solution behavior. However, in our experiments, we will concentrate more on the solution properties of the system by obtaining the characteristic Debye plot, which is C vs. KC/R_θ plot of Eq. (6). The straight line obtained from the plot gives its gradient as the second virial coefficient (a_2). From the value of a_2, we can predict the solution stability of the system. The more the a_2 value, the more is the solution stability. Similarly, the more the value of the y-intercept (i.e. $1/K_d$), less will be the molecular weight of the cluster. Hence, comparing the above two parameters, we can predict the possible mode of the Cyt-C–CdS interaction and the order of the process.

The experiment was performed with concentration of the protein nanoform complex kept a fixed mass ratio of the two 1:1. The concentration range 0.025 mg/ml to 0.25 mg/ml was suitable for construction of the Debye plot.

3.5. Scanning electron microscopy (SEM)

Microstructures of the nanoforms were obtained by scanning electron microscopy (Hitachi S-3200). The samples of protein nanoform complex were prepared in aqueous solution and then the solution was subjected to vacuum drying. Typically, the concentration of the protein and the nanoforms were varied from 0.1 mg/ml to 0.2 mg/ml (protein and nanoform kept at 1:1 mass ratio). In actual experiment, different magnifications were studied, only a few representative case being reported.

3.6. X-ray diffraction (XRD)

The products were characterized using a Seifert 3000P X-ray diffractometer with Cu Kα radiation. The nanoform and the nanoform protein complexes were studied. The samples were prepared as described in Section 3.5.

3.7. Microscopy

Slides were prepared for microscopic examination using Olympus BX51 microscope of nanoform protein complex. Three or four drops of the complex were placed on a slide and were subjected to examination by bright field microscopy. While the cluster morphology can be better seen at higher magnification (×1000), a more robust statistical distribution of the cluster was obtained at magnification (×200) using 20× objective. The image thus obtained was analyzed using Olympus MicroImage software. For evaluating the cluster distribution, the automated tracing of the cluster objects was performed and traced binary image was saved and used for general inference.

4. Results

4.1. Cytochrome C unfolding and folding pathway have been tracked by nanodeclustering

4.1.1. Tracking the temperature induced unfolding pathway

Temperature induced unfolding pathway of Cyt-C has been observed under optical microscope by following the route of cluster formation of CdSnr nanoforms. As shown in Fig. 1(a), the Cyt-C and CdSnr mixture has been heated gradually from 30 °C onwards. CdSnr only does not exhibit any major cluster alteration while responding to the heating effect (see the bottom panels of Fig. 1(a)). But the nanorods in the presence of Cyt-C behave much differently. They are observed to form small clusters in lower temperature range (30–70 °C) and their size is found to increase significantly 75 °C onwards and attains the form of giant clusters.

4.1.2. Drawing the melting curve

To get a more quantitative picture of this cluster formation, a melting curve has been constructed by performing the experiment several times, additionally taking the intermediate temperature range from 70 to 100 °C (e.g. 75, 85 and 95 °C). The cluster densities of the nanorods have been computed by using black/white pixel ratio. This cluster density (F) has been plotted against temperature axis in Fig. 1(b). This melting curve shows the transition of the cluster size being taken place between 75 and 95 °C and the middlemost point observed in this transition gives the melting point to be 89 °C, which is close to the reported melting point [31] of Cyt-C (83 °C).

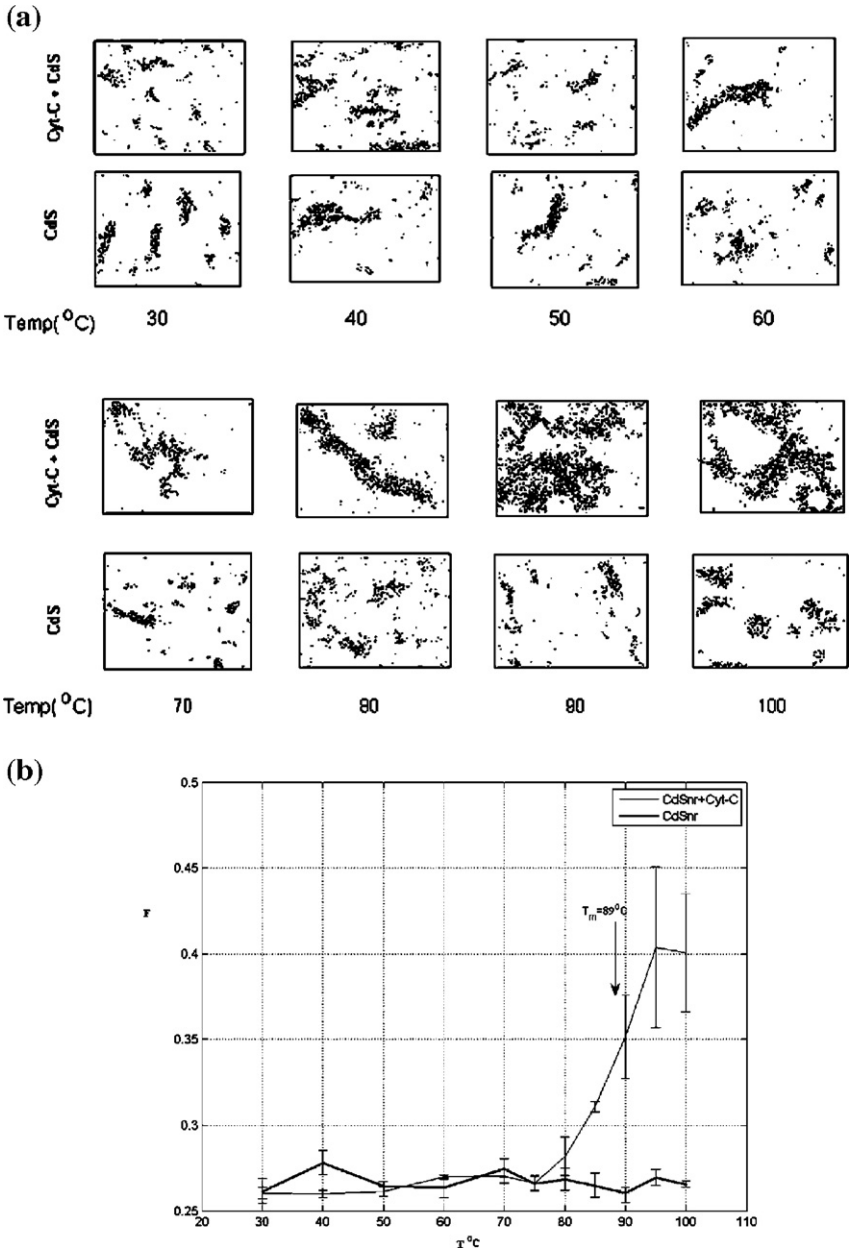

Fig. 1. (a) Temperature induced unfolding of Cyt-C tracked by cluster formation by Cdsnr. In this figure, the gradually higher order clusters are formed in CdSnr in presence of Cyt-C reflecting the unfolding induced aggregatory unfolding route of Cyt-C. But, the CdSnr itself follows no such clustering route in this temperature coordinate. This proves that the clustering phenomena is directly influenced by folding state of Cyt-C, which unfolds with increasing temperature and forms large aggregates (near 83 °C [31]). (b) The thermal melting is observed by plotting cluster density (*F*) vs. temperature (*T*, °C). *F* was calculated by computing black(cluster)/white(no cluster) pixel for each temperature snap. This plot shows a characteristic melting curve for Cyt-C having experimental Tm as 89 °C, whereas the CdSnr itself remains almost unaltered.

However, the CdSnr itself does not show such behavior (Fig. 1(b)) and almost follows a straight line through out the temperature axis. This is an effective negative control to show that temperature and illumination has no effect on the clustering of nanorods.

In addition, for CdSnr–Cyt-C mixture, the increased magnitude of the error bar in higher temperature range is attributed to the fact that with the increase of the unfolding stress, the unfolded or rather misfolded aggregates of Cyt-C forms more heterogeneous population distribution in higher temperature range and this diversity of the population is reflected in the heterogeneity of the higher order nanorod clusters, resulting in error bars with comparatively higher magnitudes in higher temperature range.

4.1.3. Construction of the Gdn–HCl induced unfolding curve of Cyt-C

Gdn–HCl induced unfolding pathway of Cyt-C has been observed by plotting the cluster density, *F* vs. Gdn–HCl molar concentration in Fig. 2a(i). The error plot hints towards a characteristic unfolding curve. The size of the CdSnr clusters in the presence of Cyt-C has been found to increase significantly

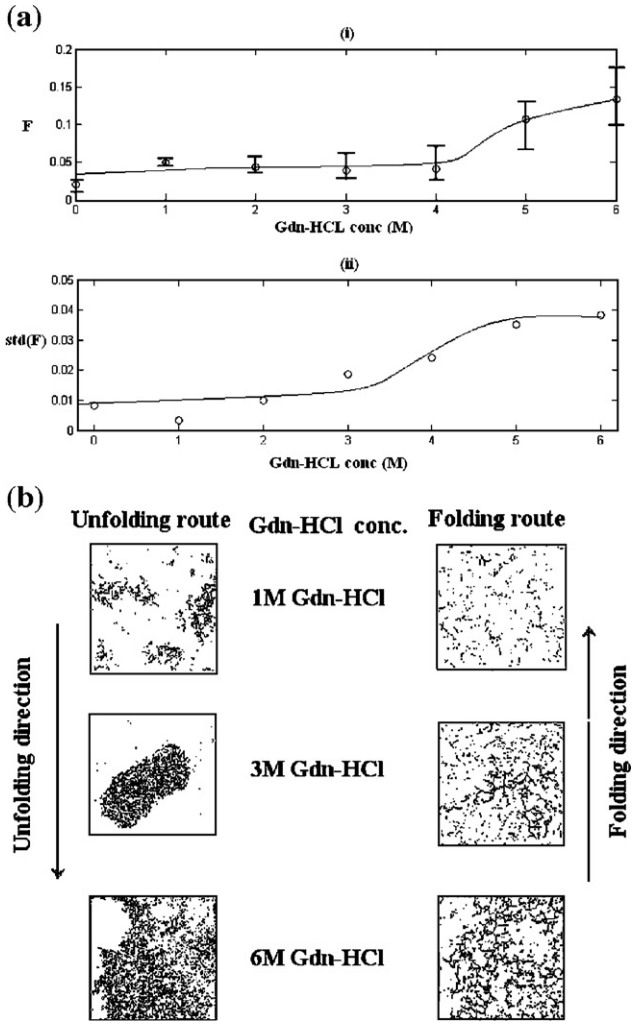

Fig. 2. (a) The Gdn–HCl induced unfolding kinetics of Cyt-C has been observed in conjugation with CdSnr. The cluster density has been plotted against Gdn–HCl concentration in (i) and the corresponding standard deviation values as a measure of population heterogeneity against Gdn–HCl concentration in (ii). (b) Refolding of Cyt-C kinetics shown by declustering of nanoforms. The left panel represents the unfolding route and the right panel shows the folding route of Cyt-C in presence of 1, 3 and 6 M Gdn–HCl concentrations. The folding route shows the dispersion of cluster connectivities and the clusters formed during folding pathway are less compact than their unfolding counterpart in left panel (i.e. same Gdn–HCl molar concentration in unfolding route).

from 4 M Gdn–HCl concentrations. A sigmoid nature is observed in the curve, hinting that the cooperativity of Cyt-C unfolding (as well as folding) has been injected in the clustering properties of CdSnr.

In addition, the standard deviation of the cluster density has also been plotted in Fig. 2a(ii) against the Gdn–HCl concentration to show that the population heterogeneity as a function of unfolding stress. This signifies that the population is becoming heterogeneous with the unfolding stress, again relating to the fact that unfolding of Cyt-C induces unfolding aggregated structures of versatile multimericity [5].

4.1.4. Differentiating between folding and unfolding pathway

Fig. 2(b) describes the declustering of CdSnr of the protein during unfolding and folding, respectively. The left panel (Fig. 2(b)) shows the clustering of CdSnr obtained by optical microscopy. Unfolding was induced by addition of various Gdn–HCl concentrations (1, 3 and 6 M). The right panel (in Fig. 2(b)) shows refolding course at equivalent Gdn–HCl concentration diluted from higher unfolding states.

Now if we compare the left (unfolding) and right (folding) panel, the only physicochemical difference between them is the pathway of reaction. The aggregating nature of unfolding pathway of Cyt-C and the deaggregating nature of the refolding pathway has been reflected on the clustering of nanorods in the left panel and declustering in the right one. Hence, the CdSnr and Cyt-C are becoming conformationally correlated in such a way that the signature of the folding state of Cyt-C is being reflected via CdSnr. So, CdSnr provides a simple visual responder of the structural changes associated with such processes. The detailed description of this interaction between protein and nanosurface will be discussed in rest of the sections.

4.2. Characterization of CdS–Cyt-C interaction

4.2.1. Cyt-C induced alteration of the distribution of CdS property matrix

Fig. 3 is the three-dimensional property matrixes of the CdS nanoclusters (both particle and rod shaped) in the presence and absence of Cyt-C obtained from the dynamic light scattering measurements. This representation of experimental data is helpful for the visualization of various populations of a particular nanocluster. The properties, which are taken as the axes of the matrix are hydrodynamic diameter (in nm) in the *x*-axis, conductance (in mS/cm) in the *y*-axis and zeta potential (in mV) in the *z*-axis. The *x*-axis, referring to the size of the cluster, is reflective of the extent of associability of monomeric population in the solution phase. For every single population of size, the corresponding conductance and zeta potential are measured. Depending on the triple axis of property, the ‘property cone’ has been constructed, whose center is the coordinates of *x*- and *y*-axes (i.e. hydrodynamic size and conductance) and height being the representative of zeta potential. Distribution of the property cones represents the nature of the diversity of the population.

Fig. 3(a) and (b) are representatives of the altered clustering of CdSnp and CdSnr, respectively, both in absence and in presence of Cyt-C. In case of both the native CdSnp and CdSnr nanoclusters’ population, the distribution is found to be very much close to each other. But, when this distribution is perturbed by the Cyt-C, the distribution becomes much diffused in the property matrix.

In Fig. 3(a), it has clearly been shown that all the three properties of CdSnp nanocluster distribution have been altered significantly and the property cones have been much more separated from each other. More importantly, the conductance of the system has been increased significantly with corresponding decrease of the zeta potential.

Similarly, in Fig. 3(b), the property cones of CdSnr have been found to be much dispersed when treated with Cyt-C. However, the resulting population is characterized by a homogenous conductance and zeta potential distribution in spite of the varying size distribution starting from as small as

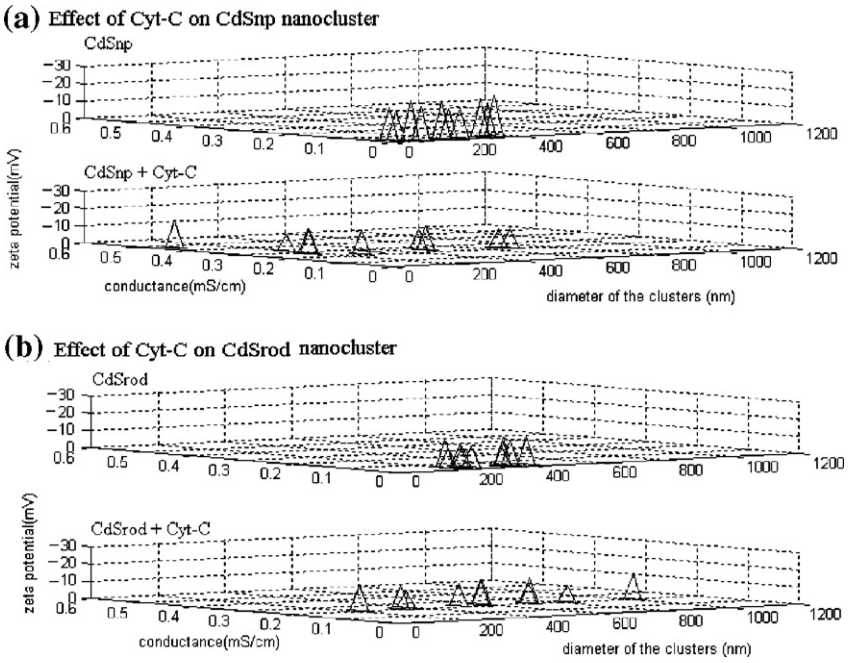

Fig. 3. Shows the effect of Cyt-C on the population distribution of CdSnp (a) and CdSnr (b) nanoclusters. Here different property cones have been constructed taking hydrodynamic diameter, conductance and zeta potential as the properties. Here, the *x*-axis denotes the hydrodynamic diameter of the clusters, *y*-axis shows the conductance and *z*-axis is the zeta potential. The dispersion of the population of the cones of CdS in presence of Cyt-C is observed in both particle (CdSnp) and rod (CdSnr) shape.

70 nm to as large as 1 μm. This indicates that in the presence of Cyt-C the nanoforms normally tend to become well dispersed.

4.2.2. SLS study to measure Cyt-C induced altered solution property of CdS nanoclusters

To answer the question whether protein covers the nanosurface or the reverse, the Debye plot of the system is obtained. As mentioned earlier, Debye plot is the plot of KC/R vs. C, which gives a straight line whose gradient is the second virial coefficient (a_2) and y-intercept being the inverse of the molecular weight. Fig. 4(a) is the Debye plot of CdSnp in the absence and in the presence of Cyt-C (in 1:1 stoichiometry) and Fig. 4(b) is the same for CdSnr system. In case of CdSnp, the value of a_2 is observed to be 0.036 unit (ml mol/g^2) and Cyt-C increases the value of a_2 by almost four times (a_2 of Cyt-C–CdSnp system is observed to be 0.14 unit). In addition, the y-intercept decreases significantly to denote the increased size of the clusters. This is supportive to the cluster dynamics data shown previously in Fig. 3.

CdSnr clusters yield a characteristic straight line with a_2 value of 0.12 unit and becomes 0.5 and 3.5 unit in the presence of low (less than 0.15 mg/ml) and high (above 0.15 mg/ml) concentration of Cyt-C. Hence, the solubility is increasing 4- to 30-fold.

This leads us to comment whether protein is covering the nanosurface. The increased solubility of the system in the presence of Cyt-C is certainly indicative of a hydrophilic layering on the surface of CdS nanoforms. This implies that Cyt-C offers its peptide framework as a cover to the CdSnr (as well as CdSnp in the earlier case) clusters resulting in enhanced solubilisation, where this hydrophilic layering is nothing but the hydrophilic amino acid residues of Cyt-C. Thus, protein is covering the nanosurface in solution phase. This will be further discussed in Section 4.2.3.

In addition to this, the influence of Cyt-C on the Debye plot of CdSnr, shown in Fig. 6(b), is rather two faced. As shown in Fig. 4(b), in the presence of Cyt-C, it shows a critical micellization type of behavior, characterized by the intersection of two straight lines near the concentration of 0.15 mg/ml, i.e. after this critical concentration the nature of CdSnr–Cyt-C

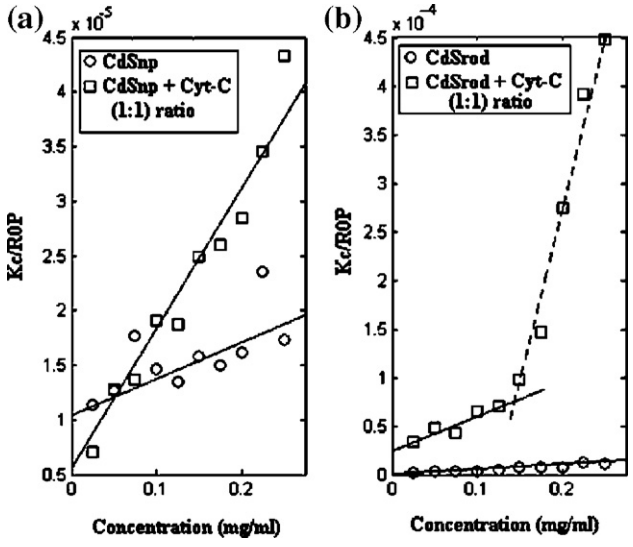

Fig. 4. Is the Debye plot of CdSnp (a) and CdSnr (b) both in absence and in presence of Cyt-C. Debye plot is the representative of the solution property of the species. Here *x*-axis is concentration (mg/ml) and *y*-axis is KC/R. This plot shows increased second virial coefficient (increased slope) indicating the more solution affinity of the nanoparticles or rods in the presence of Cyt-C.

interaction changes to influence higher order of complex formation. This is indicative of a phase change during the reaction. From the obtained a_2 values (0.5 and 3.5 unit, respectively), i.e. of the two straight lines (in low and high concentration range, respectively), it is possible that two types of interaction are present in these two concentration ranges.

4.2.3. Scanning electron microscopy shows the morphology of protein nanoparticle complex

For more precise observation of the nature of Cyt-C–CdS interaction, scanning electron microscopy (SEM) has been used. In Fig. 5, the SEM images of CdSnr have been observed in absence and in presence of Cyt-C. Fig. 5(a) and (b) are the SEM images of CdSnr and CdSnr in the presence of Cyt-C interacted with 1:1 stoichiometry, respectively. CdSnr has been observed to form layered structure with the Cyt-C peptide framework to form complex. The complex observed in Fig. 5(b) denotes a compact complex formation where the nanorods are tightly covered by the protein. Hence, Cyt-C population is forming a mesh like network, which is tightly covering the nanosurface seemingly imparting a bending stress. This is in agreement with

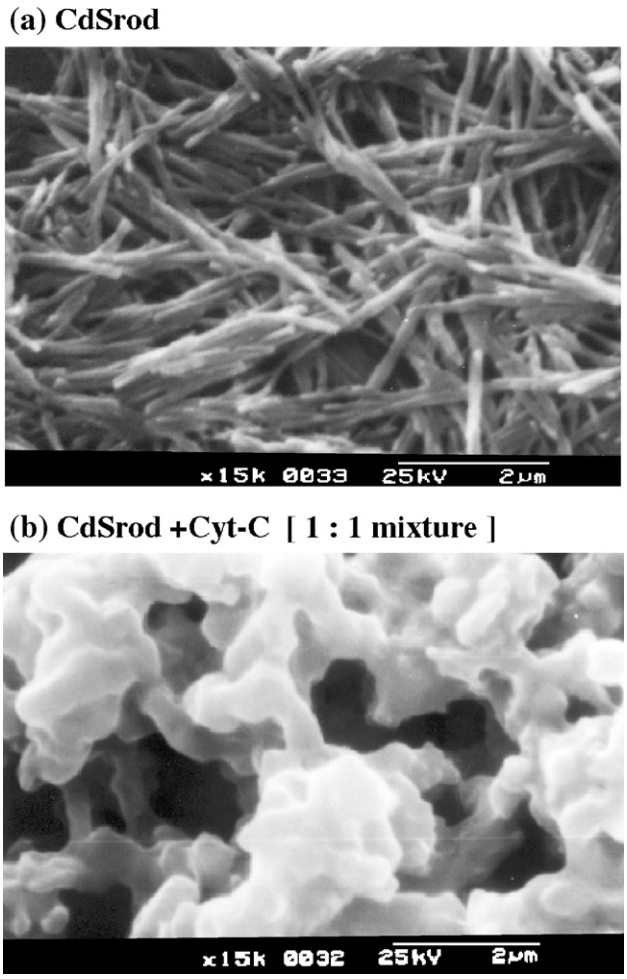

Fig. 5. Shows the SEM pictures of the complex formed by CdS Cyt-C interaction. (a) and (b) are the native forms of CdSnr and CdSnr+Cyt-C, respectively. The complex formation between CdSnr and Cyt-C is observed in the later picture.

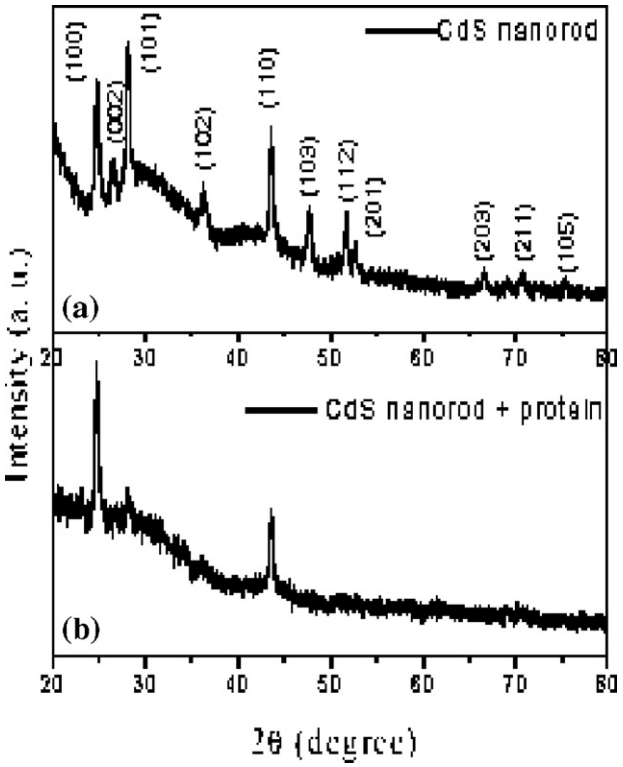

Fig. 6. XRD pattern of CdSnr in the absence (a) and in the presence (b) of Cyt-C. The pattern shows a significant change of crystal orientation has taken place in presence of Cyt-C.

Section 4.2.2, where the presence of Cyt-C was observed to increase the solubility of the system because of the protein layering on nanosurface.

However, CdSnp has shown weaker interaction in this experiment (data not shown).

4.2.4. X-ray diffraction method shows altered crystal property of CdS in presence of Cyt-C

Fig. 6(a) depicts the XRD pattern of the as prepared CdS nanorods. Fig. 6(b) illustrates the XRD profiles of CdS nanorods after its interaction with Cyt-C. Comparative study of both the XRD patterns revealed that a number of XRD peak except the peaks due to (100) and (110) planes of CdS disappeared in the presence of Cyt-C. This observation indicated a definite change in the crystallographic orientation of the CdS nanorods in the presence Cyt-C. This study thus confirmed the interaction of CdS nanorods with the Cyt-C.

5. Discussion

The work highlights interaction between Cyt-C and CdSnr. A strong coherence between the conformational dynamics of protein and nanoforms is observed. The first important observation regarding the surface attachment was that the nanosurface is coated with the hydrophilic protein exterior (leading to a positive value of second Virial coefficient). This surface adhesion was a function of the folding state of the protein.

In the absence of any nanosurface Cyt-C unfolding is characterized by formation of aggregates and its folding is

deaggregatory in nature [5]. The nanoforms participate in this population (or cluster) restructuring process both during folding and unfolding (see Fig. 3). Higher cluster density of proteins somehow imparts higher cluster density in the rods and vice versa.

This tight coupling of the cluster order of the protein and the nanorods may be made to use in tracing the melting of the protein (Fig. 2a) and maybe other changes that cause the aggregation of proteins.

The question that may be a little intriguing is that how the nanoforms, in spite of its reliable documentation of the folding state (which implies that energy minima of the protein is not appreciably affected), is undergoing some changes in its crystalline property or morphology (Figs. 5 and 6).

As we have mentioned in our previous work [5], that folding state of Cyt-C is usefully represented by its peroxidase activity. Hence, we have assayed the peroxidase activity of Cyt-C both in the absence and in the presence of CdSnp and CdSnr. The native protein shows specific activity of 2.85×10^2 units (mol *o*-dianisidine oxidized/min/mg protein). This specific activity is altered only 1.2-fold in the presence of CdSnr and 1.25-fold in the presence of CdSnp. This alteration is insignificant with the fact that in the presence of only 1 M Gdn–HCl (this concentration is very low to unfold Cyt-C) the activity increases 5-fold and higher unfolding condition like 8 M Gdn–HCl (this concentration causes large scale unfolding of Cyt-C) increases the activity by almost 40-fold [5]. This once again confirms that the perturbation of nanosurface hardly alters the folding state of Cyt-C. So, CdSnr acts only as the reporter of the Cyt-C folding state by becoming clustered or declustered in the presence of unfolded and folded protein, respectively.

6. Conclusion

The major inference that can be drawn from the present work is that one can initiate an information transfer process from protein to the nanoforms by the virtue of the folding state of the former. This information transfer is traceable by clustering and declustering of the nanoforms. The visual distinction of the folding and unfolding pathways may be one intricate feature of this cluster method, as compared to other methods (say one reported by Zare), in which a fast local equilibrium with the immediate environment would prevent the dynamic "memory" of the folding history retained by the nanoclusters. In contrary, the cluster distribution that can be traced by simple microscopy is actually a snapshot of the folding history.

Acknowledgement

We acknowledge CSIR (Council for Scientific and Industrial Research), India for the financial support during this work.

References

[1] H.S. Chung, M. Khalil, A.W. Smith, Z. Ganim, A. Tokmakoff, Conformational changes during the nanosecond-to-millisecond unfolding of ubiquitin, Proc. Natl. Acad. Sci. 102 (2005) 612–617.
[2] M.M. Pierce, T.B. Nall, Coupled kinetic traps in cytochrome *c* folding: His-Heme misligation and proline isomerization, J. Mol. Biol. 298 (2000) 955–969.
[3] M.M. Pierce, T.B. Nall, Fast folding of cytochrome *c*, Protein Sci. 6 (1997) 618–627.
[4] M. Gulotta, E. Rogatsky, R.H. Callender, R.B. Dyer, Primary folding dynamics of sperm whale apomyoglobin: core formation, Biophys. J. 84 (2003) 1909–1918.
[5] S. Roy, S. Singha, J. Bhattacharya, R. GhoshMoulick, A.K. Dasgupta, A size dependent folding contour for cytochrome-*C*, Biophys. Chemist. 119 (2006) 15–23.
[6] M.E. Dumont, J.F. Ernst, F. Sherman, Coupling of heme attachment to import of cytochrome *c* into yeast mitochondria. Studies with heme lyase-deficient mitochondria and altered apocytochromes c, J. Biol. Chem. 263 (1988) 15928–15937.
[7] P. D Barker, S.J. Ferguson, Still a puzzle: why is haem covalently attached in *c*-type cytochromes? Structure 7 (1999) 281–290.
[8] P. Garcia, M. Bruix, M. Rico, S. Ciofi-Baffoni, L. Banci, M.C.R. Shastry, H. Roder, T. de Lumley Woodyear, C.M. Johnson, A.R. Fersht, P.D. Barker, Effects of heme on the structure of the denatured state and folding kinetics of cytochrome *b*562, J. Mol. Biol. 346 (2005) 331–344.
[9] J. Bhattacharya, R. GhoshMoulick, U. Choudhuri, P.K. Bhattacharya, B. Chakrabarti, A.K. Dasgupta, Lazy dynamics of unfolding and ligand interaction-signatures of hemoglobin and its glycated form, Indian J. Phys. 78-B (2004) 55–63.
[10] M. Waks, Y.K. Yip, S. Beychok, Recombination of separated human — and β-globin chains with heme and alloplex interactions of globin chains with heme-containing subunits, J. Biol. Chem. 248 (1973) 6462.
[11] Y. Bai, Kinetic evidence for an on-pathway intermediate in the folding of cytochrome *c*, Biophysics 96 (1999) 477–480.
[12] J.R. Winkler, H.B. Gray, E.V. Pletneva, Many faces of the unfolded state: conformational heterogeneity in denatured yeast cytochrome *C*, J. Mol. Biol. 345 (2005) 855–867.
[13] J.C. Lee, H.B. Gray, J.R. Winkler, Cytochrome *c′* folding triggered by electron transfer: fast and slow formation of four-helix bundles, Proc. Natl. Acad. Sci. 98 (2001) 7760–7764.
[14] C. Du, G. Falini, S. Fermani, C. Abbott, J. Moradian-Oldak, Supramolecular assembly of amelogenin nanospheres into birefringent microribbons, Science 307 (2005) 1450–1454.
[15] S. Chah, R. Mathew, R.N. Zare, Gold nanoparticles as a colorimetric sensor for protein conformational changes, Chem. Biol. 12 (2005) 323–332.
[16] X. Jiang, J. Jiang, Y. Jin, E. Wang, S. Dong, Effect of colloidal gold size on the conformational changes of adsorbed cytochrome *c*: probing by circular dichroism, UV–visible, and infrared spectroscopy, Biomacromolecules 6 (2005) 46–53.
[17] L. Liang, P. Yao, J. Gong, M. Jiang, Interaction of apo cytochrome *c* with sulfonated polystyrene nanoparticles, Langmuir 20 (2004) 3333–3338.
[18] K. Rezwan, L.P. Meier, L.J. Gauckler, Lysozyme and bovine serum albumin adsorption on uncoated silica and AlOOH-coated silica particles: the influence of positively and negatively charged oxide surface coatings, Biomaterials 26 (2005) 4351–4357.
[19] M. Lundqvist, I. Sethson, B.H. Jonsson, High-resolution 2D 1H–15N NMR characterization of persistent structural alterations of proteins induced by interactions with silica nanoparticles, Langmuir 21 (2005) 5974–5979.
[20] M. Lundqvist, I. Sethson, B.H. Jonsson, Transient interaction with nanoparticles "freezes" a protein in an ensemble of metastable near-native conformations, Biochemistry 44 (2005) 10093–10099.
[21] F. Piazza, P. De Los Rios, Y.H. Sanejouand, Slow energy relaxation of macromolecules and nanoclusters in solution, Phys. Rev. Lett. 94 (14) (2005) 145502 (Electronic publication 2005 Apr 12).
[22] B.Q. Xu, X.L. Li, X.Y. Xiao, H. Sakaguchi, N.J. Tao, Electromechanical and conductance switching properties of single oligothiophene molecules, Nano Lett. 5 (2005) 1491–1495.
[23] A.T. Chan, J.A. Lewis, Electrostatically tuned interactions in silica microsphere-polystyrene nanoparticle mixtures, Langmuir 21 (2005) 8576–8579.

[24] H. Zhou, X. Gan, T. Liu, Q. Yang, G. Li, Effect of nano cadmium sulfide on the electron transfer reactivity and peroxidase activity of hemoglobin, J. Biochem. Biophys. Methods 64 (2005) 38–45.
[25] J.J. Valente, K.S. Verma, M.C. Manning, W.W. Wilson, C.S. Henry, Second virial coefficient studies of cosolvent induced protein self-interaction, Biophys. J. (2005) (Sep 30; [Electronic publication ahead of print]).
[26] A. Paliwal, D. Asthagiri, D. Abras, A.M. Lenhoff, M.E. Paulaitis, Light-scattering studies of protein solutions: role of hydration in weak protein–protein interactions, Biophys. J. 89 (2005) 1564–1573.
[27] S. Kar, S.K. Panda, B. Satpati, P.V. Satyam, S. Chaudhuri, Morphology and size dependent optical properties of CdS in different nanoforms, J. Nanosci. Nanotechnol. 6 (2006) 771–776.
[28] N. Griffon, V. Baudin, W. Dieryck, A. Dumoulin, J. Pagnier, C. Poyart, M. C. Maeden, Tetramer–dimer equilibrium of oxyhemoglobin mutants determined from auto oxidation rates, Protein Sci. 7 (1998) 673–680.
[29] P. Hensley, K. Moffat, S.J. Edelstein, Influence of inositol hexaphosphate binding on subunit dissociation in methemoglobin, J. Biol. Chem. 250 (1975) 9391–9396.
[30] M. Hidvegi, R. Lasztity, Phytic acid content of cereals and legumes and interaction with proteins, Period. Polytech., Ser. Chem. 46 (2002) 59–64.
[31] A. Muga, H.H. Mantsch, W.K. Surewicz, Membrane binding induces destabilization of cytochrome *c* structure, Biochemistry 30 (1991) 7219–7224.